ORIGINAL CONTRIBUTION

Pressure-driven pipe flow of semi-dilute and dense suspensions over permeable surfaces

Changwoo Kang[1,2] · Parisa Mirbod[1]

Abstract

We study pressure-driven suspensions of non-colloidal, non-Brownian, and rigid spheres in a Newtonian solvent where the pipe surface is replaced by porous media using numerical simulations. We examine various values of the permeability of the porous medium K, while we keep the porosity and the thickness of the porous layer constant to clarify the effect of the permeable wall on the suspension flows at bulk particle volume fractions $0.1 \leq \phi_b \leq 0.5$. In the limit of vanishing inertia, the rate of suspension flow decreases as the bulk volume fraction ϕ_b increases and it builds up as the permeability of the porous media increases. There are also two different regimes characterizing the dimensionless slip velocity normalized by both shear rate and penetration depth, namely, the strong permeability regime and the weak permeability regime. In the former, the solvent penetrates deeper and the streamwise velocity at the interface increases with the porous media permeability, while in the latter, the fluid cannot go through the porous media deeply and the variation of the slip velocity with the permeability is small. Our results might suggest a new passive technique to reduce drag by enhancing the rate of suspension flow in devices where the suspension transport is crucial. It might also offer basic insights for the extension to the flow of suspensions over and through complex porous media.

Introduction

Reducing dissipation and drag in flows enclosed by solid boundaries and therefore, fabricating economically advanced and efficient devices has attracted more attentions over the past decades. Previous studies have shown that, in the case of rigid superhydrophobic surfaces, the slip of the fluid greatly increases the rate of Newtonian fluid flow, potentially resolving the issue of the very high hydrodynamic drag in microfluidic devices.

Complex fluids, on the other hand, are encountered in many industries including micro-fluidic devices, biological systems, food-processing, pharmaceutical industries. In these applications, being able to control the boundary conditions plays a major role in driving and controlling the flow. Moreover, understanding the boundary conditions of complex fluids at solid surfaces sheds light on these flows at the interfaces, which is critical in fluid dynamics. Extensive works on Newtonian liquid flows over a stationary surface where the slip boundary condition including superhydrophobic surfaces and polymer brushes applied at the surface have been performed (Guo et al. 2000; Kruijt et al. 2000; Tachie et al. 2004; Goharzadeh et al. 2005; Ghisalberti and Nepf 2009; Battiato et al. 2010; Deng et al. 2012; and references therein). Here, however, we characterize the flow and the rate of particle-laden liquids flow, where the permeable surfaces exist, and correlate the characteristics of the suspension flow to the geometry of the device.

One of the useful ways to understand the rheology of complex fluids is by modeling them as suspensions of particles in a Newtonian solvent with viscosity η_f and density ρ_f. Two different continuum models have been developed to describe the dynamics of suspension flows. The first model, the diffusive flux model (DFM), introduced by Leighton and Acrivos (1987) and later by Phillips et al. (1992), is phenomenological and involves the diffusion fluxes of particles due to particle collisions and the spatial variation in the viscosity. The second

✉ Parisa Mirbod
pmirbod@uic.edu

1 Department of Mechanical and Industrial Engineering, University of Illinois at Chicago, 842 W. Taylor Street, Chicago, IL 60607, USA

2 Department of Mechanical Engineering, Jeonbuk National University, 567 Baekje-daero, Deokjin-gu, Jeonju-si, Jeollabuk-do 54896, Republic of Korea

model, the suspension balance model (SBM) (Jenkins and McTigue 1990; Nott and Brady 1994), is rooted in the conservation equations of mass, momentum, and energy for the fluid and particle phases. These models have mostly succeeded in predicting qualitative features of the migration process and quantitative steady-state velocity and concentration profiles for different pressure-driven and shear flows in a channel, pipe, and Couette geometries (Phillips et al. 1992; Nott and Brady 1994; Subia et al. 1998; Morris and Brady 1998; Morris and Boulay 1999; Fang et al. 2002; Miller and Morris 2006; Ahmed and Singh 2011; Dbouk et al. 2013; Mirbod 2016; Chun et al. 2019).

In this study, while keeping small Reynolds number, we focus on examining the flow of particulate suspensions in a pipe with radius R where its walls are replaced with a permeable surface with known physical properties including permeability K, porosity ε, and thickness h (Fig. 1). Specifically, we explore non-colloidal, non-Brownian suspensions of rigid and spherical particles of bulk concentration ϕ_b in a Newtonian fluid over a wide range of particle volume fraction (i.e., ϕ_b=10% to 50%). We introduce three different dimensionless parameters; the permeability parameter $\sigma = R/\sqrt{K}$, the depth ratio $\delta = h/R$, and the particle volume fraction ϕ_b. The problem of 2D steady-state non-Brownian suspension pipe flow with impermeable walls (i.e., $\sigma \rightarrow 0$) has a long history pioneered with the work by Karnis et al. (1966) and later by Leighton and Acrivos (1987), Altobelli et al. (1991), Sinton and Chow (1991), and Phillips et al. (1992) who showed that for high ϕ_b, the velocity profile was flattened in the center compare to the parabolic velocity profile obtained for a pure Newtonian fluid with the same average material properties. Several researchers extensively have examined dilute and concentrated non-Brownian, non-colloidal suspension flows of channel and pipe both numerically and experimentally (Koh et al. 1994; Hampton et al. 1997; Han et al. 1997; Subia et al. 1998; Lyon and Leal 1998a, b; Ahmed and Singh 2011; Chun et al. 2019).
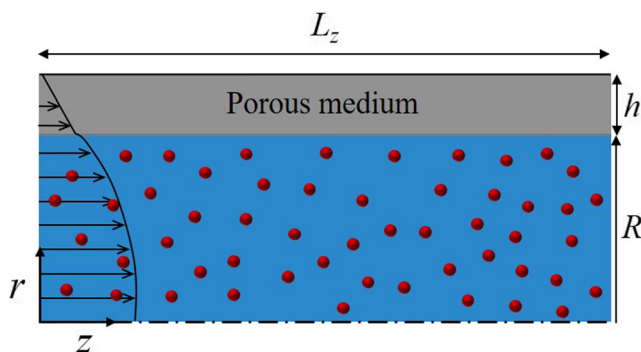
Fig. 1 Schematic diagram of a circular Poiseuille flow of suspensions in a pipe over a permeable surface with permeability K and thickness h (= 0.2R). Arrows indicate the flow direction and a sketch of the velocity profile

Due to the simplicity, low computational cost, and good accuracy of the constitutive model reported in Phillips et al. (1992), i.e., DFM, in this work to analytically model the flow of suspensions, we couple the DFM with Darcy's law (Darcy 1856) in a porous medium. Numerical simulations are conducted to solve conservation equations of the flow coupled with the constitutive equation of suspensions. We aim to elucidate the effect of the permeable surface on the suspension flows. The velocity and concentration profiles are presented for various control parameters which indicate properties of the particle volume fraction and porous surface. The velocity parameters that characterize the penetration of the flow through porous media are obtained for various values of control parameter. Furthermore, we evaluate the rate of suspension flows and slip velocity at the suspension-porous interface induced by the permeable surface.

Problem formulation

We conduct numerical simulations in the pressure-driven flow of neutrally buoyant and non-colloidal particles concentrated in an incompressible Newtonian viscous fluid in a pipe with the radius R. The suspension flows over a porous wall with the thickness h driving by a constant pressure gradient (dp/dz) in the axial z direction (see Fig. 1). We assume that the porous medium is homogeneous and isotropic and also saturated by the same fluid, i.e., constant permeability K and porosity n. While we vary the permeability of porous media, we keep constant porosity $n = 1.0$. In fact, the porosity can be a control parameter of the flow over a permeable surface (Kang and Mirbod 2019). Herein, we assumed a constant porosity ($n =$ 1.0) to simplify the problem, following previous studies (Vafai and Kim 1990, Goyeau et al. 2003), since there are several parameters (e.g., depth ratio, particle volume fraction, permeability, and porosity) that all vary and are critical in this study. It is also assumed that the size of particles is larger than the pore size of the porous medium. Therefore, particles do not penetrate into the porous region and they exist only in the fluid layer. Moreover, we suppose the Reynolds number is sufficiently small ($Re \ll 1$) in suspensions where the inertia can be neglected.

The equations of continuity and momentum for the flow of suspensions by applying a volume averaging approach can be given by Kang and Mirbod (2020).

$$\nabla \cdot \mathbf{u} = 0 \tag{1}$$

$$\rho\left(\frac{\partial \mathbf{u}}{\partial t} + \nabla \cdot (\mathbf{u}\mathbf{u})\right) = -\nabla p + \nabla \cdot (2\eta(\phi)\mathbf{S}) \tag{2}$$

Here $\mathbf{u}$, p, and ρ are the volume averaged velocity vector (u_r, u_z), pressure, and density of the fluid, respectively. $\mathbf{S} = \frac{1}{2}$

$(\nabla \mathbf{u} + \nabla \mathbf{u}^T)$ is the strain rate tensor. $\eta(\phi)$ is the viscosity of concentrated suspensions which depends on the particle volume fraction ϕ and can be described by the Krieger's empirical correlation (Krieger 1972) as $\eta(\phi) = \eta_o(1 - \phi/\phi_m)^{-1.82}$. Here, η_o is the viscosity of the suspending fluid and $\phi_m = 0.68$ is the maximum volume fraction (Krieger 1972; Phillips et al. 1992).

For the flow of a pure fluid in the porous layer, the governing equations are stated as (Kang and Mirbod 2019; Wu and Mirbod 2018; Wu and Mirbod 2019; Haffner and Mirbod 2020)

$$\nabla \cdot \mathbf{u} = 0 \tag{3}$$

$$\rho\left(\frac{\partial \mathbf{u}}{\partial t} + \nabla \cdot (\mathbf{uu})\right) = -\nabla p + \nabla \cdot (2\eta_o \mathbf{S}) - \frac{\eta_o}{K}\mathbf{u} \tag{4}$$

The last term in the right-hand-side of Eq. (4) indicates Darcy's law that represents the average of microscopic (pore-level) flow resistance (Darcy 1856; Brinkman 1949).

Using the diffusive flux model (DFM) (Leighton and Acrivos 1987; Phillips et al. 1992), the conservation equation for non-colloidal particles in a Lagrangian frame can be expressed as (Phillips et al. 1992)

$$\frac{\partial \phi}{\partial t} + \mathbf{u} \cdot \nabla \phi = -\nabla \cdot (\mathbf{N}_c + \mathbf{N}_\eta) \tag{5}$$

where $\mathbf{N}_c$ and $\mathbf{N}_\eta$ are the particle fluxes caused by spatial variation in the collision frequency and suspension viscosity, respectively, given by $N_c = -K_c a^2 \phi \nabla(\dot{\gamma}\phi)$ and $\boldsymbol{N}_\eta = -K_\eta a^2 \dot{\gamma}\phi^2 \nabla(\ln \eta)$ (Phillips et al. 1992; Subia et al. 1998). Here, a is the radius of particles and $\dot{\gamma}$ is the local shear rate given by $\dot{\gamma} = \sqrt{2\mathbf{S}:\mathbf{S}}$. Diffusion coefficient K_c and K_η are empirical constants determined by experiments. We use $K_c = 0.41$ and $K_\eta = 0.62$ ($K_c/K_\eta = 0.66$) (Phillips et al. 1992). We have also applied the nonlocal stress model on particle fluxes suggested by Miller and Morris (2006) as $\dot{\gamma}_{NL} = a_s(\epsilon)\dot{\gamma}_s$ (i.e., $\boldsymbol{N}_c = -K_c a^2 \phi \nabla\left[\left(\dot{\gamma} + \dot{\gamma}_{NL}\right)\phi\right]$ and $\boldsymbol{N}_\eta = -K_\eta a^2 \left(\dot{\gamma} + \dot{\gamma}_{NL}\right)\phi^2 \nabla(\ln \eta)$) to resolve the numerical difficulties at point where the local shear rate approaches zero at the center of pipe. Here, $a_s(\epsilon) = \epsilon$ has been chosen by the examination where $\epsilon = a/R$. $\dot{\gamma}_s = U_{max}/R$ has been used for the pipe flow with a no-slip condition on the wall, where U_{max} is the centerline velocity (Miller and Morris 2006). As denoted in Miller and Morris (2006), the finite $\dot{\gamma}_{NL}$ values are very small compared to the local shear rate ($\dot{\gamma}_{NL} \ll \dot{\gamma}$) except where $\dot{\gamma} \to 0$. Therefore, it gives the model the desired effect of influencing results only near the centerline.

The governing equations (Eqs. (1) ~ (5)) are discretized using a finite volume method in a cylindrical coordinate system. A second-order central difference scheme is used for spatial discretization of derivatives except for the convective term ($\mathbf{u} \cdot \nabla \phi$) of the conservation equation for particles (Eq. (5)), where we employed the QUICK (quadratic upstream interpolation for convective kinematics) scheme for the discretization. A hybrid scheme is utilized for time advancement, nonlinear terms are explicitly advanced by a third-order Runge-Kutta scheme, and the other terms are implicitly advanced by the Crank-Nicolson method (Kang and Yang 2011, 2012). A fractional-step method is applied for time integration. Then, the Poisson equation resulted from the second stage of the fractional step method is solved by a fast Fourier transform (FFT) (Kim and Moin 1985).

The no-slip condition is imposed on an impermeable wall ($r = R + h$), and the flow is assumed to be periodic in the axial direction (z). We assume that velocity and shear stress at the interface are continuous (Vafai and Kim 1990) and particles do not penetrate into a porous medium. Therefore, total particle flux is zero at the interface between suspending fluid and porous layer. The number of grid points determined by a grid test is $192(r) \times 64(z)$ with the axial length of the domain $L_z = 4R$. Practically, we found the error within 1% in the concentration distribution compared with those of $128(r) \times 64(z)$ and $256(r) \times 64(z)$. More grid points are allocated near impermeable wall and interface between two layers in the radial direction (r) with $\Delta r_{min} = 0.005R$, while the grid cell in the axial direction (z) is uniform. The radius of particles is $a = 0.0625R$. We choose the radius of the pipe R as the scale for length and $U_o = (-dp/dz)R^2/8\eta_o$ as the scale for velocity. The dimensionless permeability can then be defined as $\sigma = R/\sqrt{K}$ that varies from 1 to 50 in this study. Here, $\sigma = \infty$ (i.e., $K = 0$) represents the impermeable wall. The parameter $\delta = h/R$ specifies the dimensionless thickness ratio. In all of our analysis in this study, we consider δ constant equal to 0.2 by referring to the study in Guo et al. (2000) who characterized the pure Newtonian fluid in a pipe replaced with a uniform thickness of $\delta = 0.181$. Herein, the bulk concentration ϕ_b varies from 10 to 50%.

To validate our code, we compared the distributions of volume fraction (ϕ) and axial velocity component (u_z) for the flow of non-Brownian and non-colloidal suspensions with a smooth (impermeable) wall with available experimental and theoretical data in Fig. 2. Our profiles of ϕ and u_z for $\phi_b = 0.2$ and 0.3 show excellent agreement with the measurements obtained using nuclear magnetic resonance (NMR) imaging (Hampton et al. 1997) and those predicted by the DFM (Hampton et al. 1997) and SBM (Fang et al. 2002). In particular, our distributions of ϕ reveal more similar behavior to experimental observations of Hampton et al. (1997) near the center of the pipe ($r = 0$). This results from the nonlocal stress contribution ($\dot{\gamma}_{NL}$). The nonlocal stress model employed in particle fluxes causes a gentle variation of the concentration
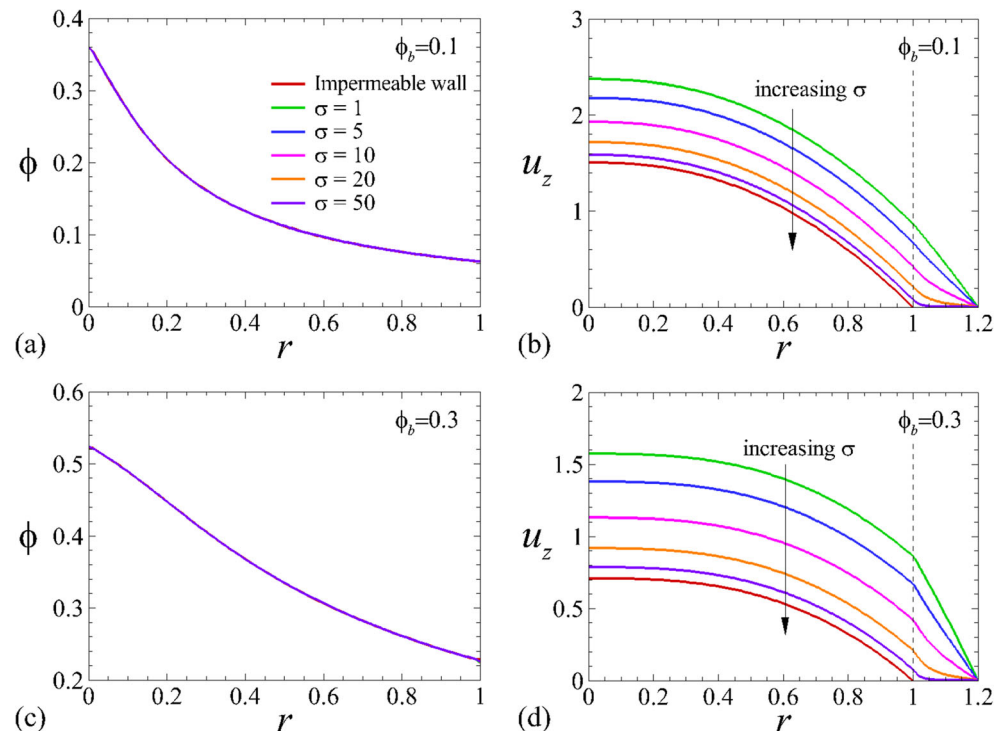
Fig. 2 Comparison of particle volume fraction (ϕ) and axial velocity (u_z) profiles of pressure-driven pipe flow of concentrated suspensions with a smooth wall for $\epsilon = 0.0625$. ϵ ($= a/R$) is the particle radius a to the radius of the pipe R, and ϕ_b is the bulk concentration. The velocity was normalized by the bulk velocity $U_b = \frac{1}{A}\int u_z dA$ where $dA = 2\pi r dr$
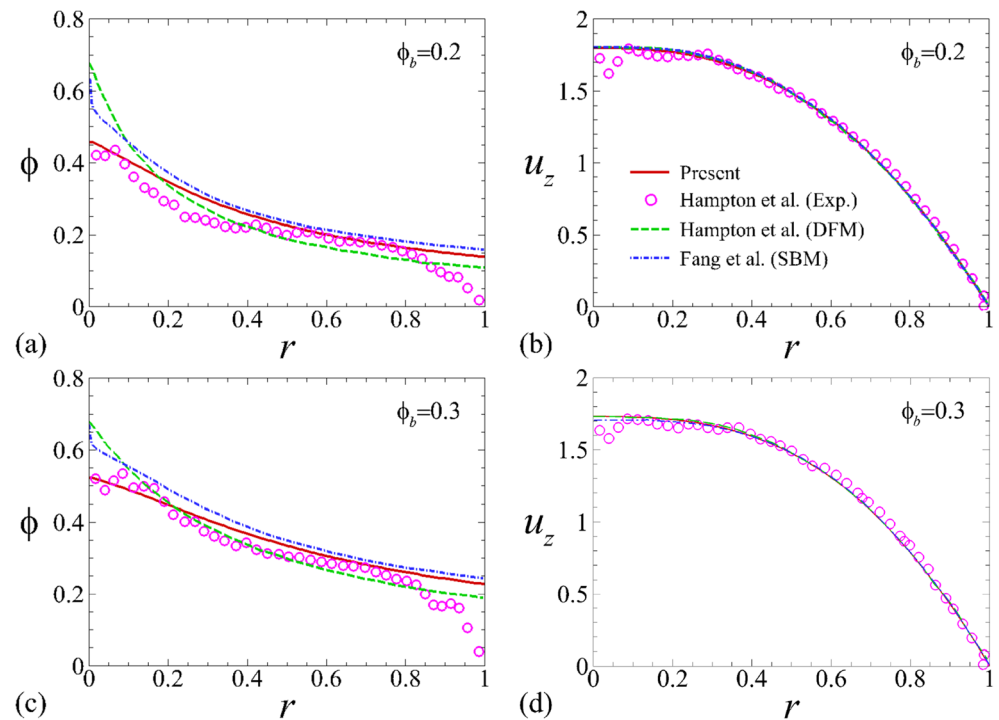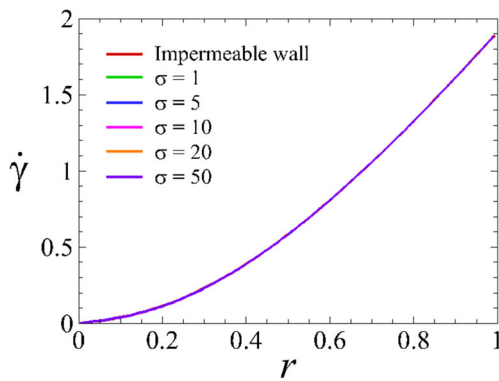
profile ϕ at the center where a sharp cusp appears without the nonlocal stress correction. It should be noted that the fluctuations at the center of the pipe seen in the experiments are due to the noise and artifacts in the NMR images (Hampton et al. 1997). Nevertheless, our result still has a little bit of discrepancy near the wall as predicted in previous theories (Hampton et al. 1997; Lyon and Leal 1998a; Fang et al. 2002; Miller and

Morris 2006). This is due to the fact that the continuum approach does not describe the physical constraint at the wall properly; therefore, the value of concentration has to drop to zero near the wall. In addition, the axial velocity (u_z) reduces with the presence of particles. It also decreases as the bulk concentration (ϕ_b) increases. Note that the maximum value of the velocity at the center for a pure Newtonian fluid is 2.0.

Fig. 3 Profiles of particle volume fraction ϕ and axial velocity component u_z normalized by U_o for various σ at $\phi_b= 0.1$ and $\phi_b= 0.3$. Dashed lines indicate the interface between suspending fluid and porous layer
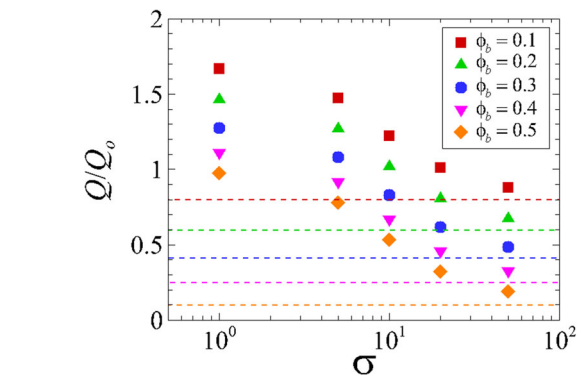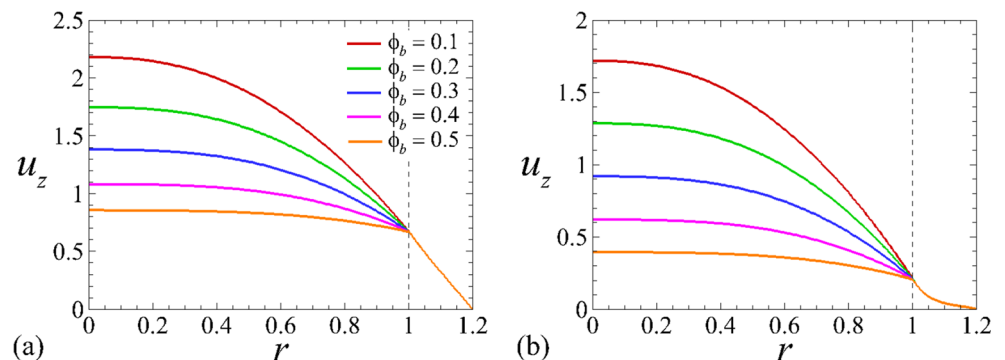
**Fig. 4** Profiles of normalized local shear rate for ϕ_b= 0.3 in the suspension region

Fig. 6 Variations of the rate of suspension flow Q for all values of ϕ_b and σ. Dashed lines represent values of suspensions over an impermeable wall Q_s/Q_o for each ϕ_b

Results and discussion

We first calculate the profiles of concentration ϕ and axial velocity u_z for various values of σ. Profiles of particle volume fraction ϕ and axial velocity component u_z normalized by U_o for various σ at ϕ_b= 0.1 and ϕ_b= 0.3 are shown in Fig. 3. Clearly, the permeable wall does not alter the distribution of concentration in the suspension region (Fig. 3(a), (c)), while it makes a noticeable change in the velocity profile (Fig. 3(b), (d)) due to the impact of the slip boundary condition caused by the permeable wall. Noted that the stress distribution at the porous-suspension interface is specified by a force balance which is linear at all concentrations; therefore, the particle concentration distribution is only dependent on the bulk concentration and the porous layer has no impact. By increasing σ (i.e., decreasing the permeability K), the velocity diminishes because the lower permeability decreases the velocity at the suspension-porous interface as well as in the porous layer by stronger viscous drag originated from Darcy's law, whereas the velocity is larger than that of suspension flows past impermeable walls even for very high σ (i.e., low permeability). As reported in Mirbod et al. (2017), Wu and Mirbod (2018), and Haffner and Mirbod (2020), the flow of pure Newtonian fluid in the fluid layer is also enhanced by the presence of a permeable wall.

We further calculate the local shear rate $\dot{\gamma}$ for various σ at ϕ_b= 0.3 in Fig. 4. As can be seen, the local shear rate $\dot{\gamma}$ is invariant in the suspension region even though the velocity rises. As observed previously (Gadala-Maria and Acrivos 1980; Goto and Kuno 1982; Leighton and Acrivos 1987; Phillips et al. 1992), for very low Re where the inertial effects are neglected, the particle migration is induced by the shear rate that migrates particles from regions of higher shear rate to regions of lower shear rate. This also confirms no variation in particle migration as has been observed in Fig. 3(a), (c). Accordingly, it reveals that the permeable wall can enhance the velocity without any change in the particle distribution.

The plots of the axial velocity profiles for various ϕ_b and σ are shown in Fig. 5. For higher bulk concentrations, due to the increase in the viscous force exerted on the fluid by the particles, the velocity in the suspension region decays. Recently, for pressure-driven flow of a pure fluid over permeable surfaces, Kang and Mirbod (2019) showed that the kinetic energy is mainly produced by the velocity-pressure gradient and it is balanced by the viscous diffusion and dissipation in the fluid layer. In this study, higher bulk concentrations trigger higher viscosity of concentrated suspensions ($\eta(\phi)$); then, stronger viscous forces are induced. As a result, the flow decays in the suspension layer. On the other hand, the velocity inside the porous region depends only on the permeability in the

Fig. 5 Profiles of axial velocity component u_z normalized by U_o for various ϕ_b; (a) $\sigma = 5$, (b) $\sigma = 20$. Dashed lines indicate the interface between suspending fluid and porous layer

Fig. 7 Variations of the slip velocity U_s, normalized by U_o and shear rate $\dot{\gamma}$, at the suspension-porous interface (i.e., $r = 1$) for all values of ϕ_b and σ
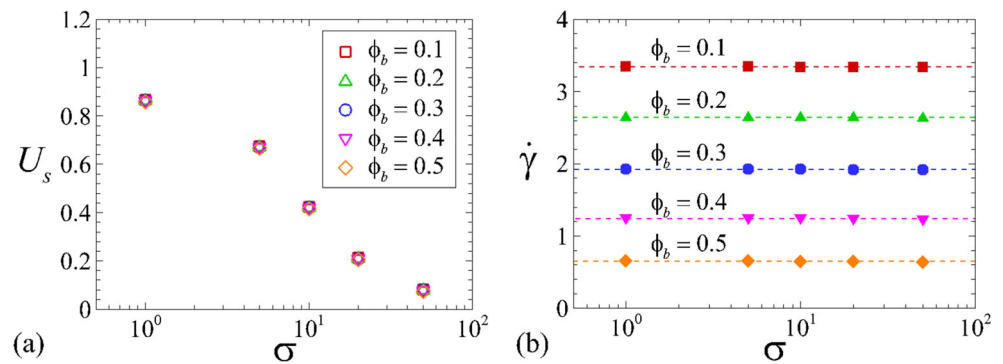

porous region and the slip velocity at the suspension-porous interface is constant. As mentioned before, this is because we assumed particles do not penetrate into the porous medium. Consequently, the flow inside the porous layer is governed by the interface shear stress as well as its properties where the suspension has no impact.

To quantify the enhancement of suspension flows induced by the permeable wall, we then estimate the volume flow rate $Q = \int_0^R u_z dA$ in the suspension flow region and compute Q for all ϕ_b and σ to plot $Q(\phi_b, \sigma)$ in Fig. 6. It should be noted that in the present study, we only evaluate the flow rate inside the suspension region because (1) our focus is on examining the impact of the permeable surface on the suspensions, and (2) as suggested by Guo et al. (2000), for $\delta = 0.2$, the flow flux passing through the porous layer can be neglected. We then normalize Q by the volume flow rate in the flow of a pure fluid over an impermeable wall (i.e., $Q_o = Q(\phi = 0, \sigma = \infty)$). As mentioned earlier, the volume flow rate decreases by increasing ϕ_b and σ. However, it is still higher than that of suspension flows over an impermeable wall, i.e., $Q_s = Q(\phi_b, \sigma = \infty)$ indicated by dashed lines in Fig. 6, even for a very low value of the permeability at $\sigma = 50$.

For the fluid flow through porous media, the slip velocity U_s defined as the streamwise (or axial) velocity at the interface is the most important parameter of the flow since it is required to evaluate the penetration of the fluid region into the porous medium (Agelinchaab et al. 2006; Arthur et al. 2009; Mirbod et al. 2017; Wu and Mirbod (2018); Wu and Mirbod (2019); Haffner and Mirbod (2020)). To characterize the variation of the slip velocity U_s normalized by U_o and shear rate $\dot{\gamma}$ at the suspension-porous interface, we then calculate U_s for all values of ϕ_b and σ; the plots of $U_s (\phi_b, \sigma)$ are shown in Fig. 7. As can be seen from this figure, U_s is independent of ϕ_b and decays as the permeability decreases (i.e., σ increases). In addition, $\dot{\gamma}$ at the interface has almost constant values for each ϕ_b regardless of σ as displayed in Fig. 4. As mentioned before, this is because of the continuous conditions of velocity and shear stress at the interface. We then examined the slip velocity with respect to another dimensionless parameter normalized by the product of the square root of the specific Darcy

permeability of the porous medium and shear rate at the interface $\dot{\gamma}\sqrt{K}$. This is a more useful dimensionless slip parameter because of its dependence on local conditions not the velocity in the suspension flow region U_o. Moreover, $U_s/\dot{\gamma}\sqrt{K}$ is equivalent to the inverse of the slip coefficient α proposed by Beavers and Joseph (1967) which is a dimensionless parameter depending on the material properties and specifies the boundary condition at the free flow-permeable interface. It can be also related to the Brinkman equation given as $\eta_{eff}\nabla^2\mathbf{u} - \nabla p - \eta_o K^{-1}\mathbf{u} = 0$ (Brinkman 1949) where the analytical solution of the shear rate at the interface is similar to the solution of Beavers and Joseph (1967) considering that $\alpha = (\eta_{eff}/\eta_o)^{1/2}$. Note that $\sqrt{K}$ states the penetration distance of the suspending fluid inside the porous media. The values of $U_s/\dot{\gamma}\sqrt{K}$ for all values of ϕ_b and σ are plotted in Fig. 8. These results reveal that the dimensionless slip parameter (or slip coefficient) is also dependent on ϕ_b. Moreover, it turns out that when the depth ratio $\delta = h/R = 0.2$ and $n = 1$, there are two different regimes characterizing the normalized slip velocity $U_s/\dot{\gamma}\sqrt{K}$, at the suspension-porous interface, namely, the strong permeability regime and the weak permeability regime. In the former, the solvent penetrates deeper and the slip velocity increases with the permeability of porous media, while in the latter, the fluid cannot go through the porous media truly and the variation of slip velocity with the permeability is small.
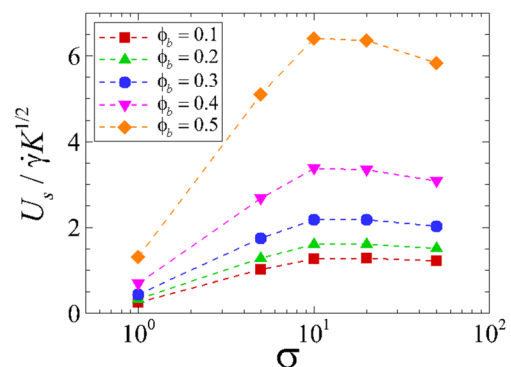
Fig. 8 Variation of $U_s/\dot{\gamma}K^{1/2}$ for all values of ϕ_b and σ

Conclusion

To conclude, our simulations show that for the pressure-driven flow of concentrated non-colloidal suspensions over a porous material in a pipe (where the particles are not moving inside the porous surface), the permeable surface does not have any impact on the concentration distribution of suspensions, whereas the velocity of suspensions enhances by the "slip" effect at the suspension-porous interface. We have also evaluated the volume flow rate in the suspension region induced by a permeable wall. We showed that the flow rate builds up by increasing the permeability and enhances for all values of σ. The slip velocity U_s and shear rate $\dot{\gamma}$ at the interface have been obtained to assess the penetration of the suspending fluid region into the porous layer. U_s depends only on σ and decreases by increasing σ. This effect for the slip velocity has also been observed in Rosti et al. (2021) for suspensions over porous media in a Couette flow using a different numerical method. The local shear rate, on the other hand, is invariant with respect to σ and it is constant for all values of ϕ_b. The normalized slip velocity $U_s/\dot{\gamma}\sqrt{K}$ is relative to ϕ_b and has the maximum value at $\sigma = 10$ for $\delta = 0.2$ and porosity of porous media $n = 1$. It is anticipated that understanding the coupling performance of suspension flows and permeable media will open up new avenue of research and provide valuable insights into improving efficiencies and operating lifetime in a wide range of microfluidic-based devices and processes related to suspension transport including biomedical fields and chemical synthesis. Our study reveals that a permeable media with a known permeability and porosity can indeed be used as a promising way toward reducing dissipation and drag in devices that use particle-laden liquids in geometries including pipes with very low suspension flow resistance; therefore, a new passive technique for enhancing the flow rate in such devices. Furthermore, the model will reveal the relation between the flow condition, permeable wall structure and properties with the geometry of the device. Future studies shall focus on the development of experimentally validated models to provide more insights into capability of DFM for suspension flows in geometries where porous media presents.

Declarations

Competing interests The authors declare no competing interests.

References

Agelinchaab M, Tachie MF, Ruth DW (2006) Velocity measurement of flow through a model three-dimensional porous medium. Phys Fluids 18:017105. https://doi.org/10.1063/1.2164847

Ahmed GMY, Singh A (2011) Numerical simulation of particle migration in asymmetric bifurcation channel. J Non-Newton Fluid 166: 42–51. https://doi.org/10.1016/j.jnnfm.2010.10.004

Altobelli SA, Givler RC, Fukushima E (1991) Velocity and concentration measurements of suspensions by nuclear magnetic resonance imaging. J Rheol 35:721–734. https://doi.org/10.1122/1.550156

Arthur JK, Ruth DW, Tachie MF (2009) PIV measurements of flow through a model porous medium with varying boundary conditions. J Fluid Mech 629:343–374. https://doi.org/10.1017/S0022112009006405

Battiato I, Bandaru PR, Tartakovsky DM (2010) Elastic response of carbon nanotube forests to aerodynamic stresses. Phys Rev Lett 105: 144504. https://doi.org/10.1103/PhysRevLett.105.144504

Beavers GS, Joseph DD (1967) Boundary conditions at a naturally permeable wall. J Fluid Mech 30:197–207. https://doi.org/10.1017/S0022112067001375

Brinkman HC (1949) A calculation of the viscous force exerted by a flowing fluid on a dense swarm of particles. App Sci Res 1:27. https://doi.org/10.1007/BF02120313

Chun B, Park JS, Jung HW, Won YY (2019) Shear-induce particle migration and segregation in non-Brownian bidisperse suspensions under planar Poiseuille flow. J Rheol 63:437–453. https://doi.org/10.1122/1.5065406

Darcy HPG (1856) Les Fontaines Publique de la Ville de Dijon. Victor Dalmont, Paris

Dbouk T, Lemaire E, Lobry L, Moukalled F (2013) Shear-induced particle migration: Predictions from experimental evaluation of the particle stress tensor. J Non-Newton Fluid 198:78–95. https://doi.org/10.1016/j.jnnfm.2013.03.006

Deng M, Li X, Liang H, Caswell B (2012) Simulation and modelling of slip flow over surfaces grafted with polymer brushes and glycocalyx fibres. J Fluid Mech 711:192–211. https://doi.org/10.1017/jfm.2012.387

Fang Z, Mammoli AA, Brady JF, Ingber MS, Mondy LA, Graham AL (2002) Flow-aligned tensor models for suspension flows. Int J Multiphase Flow 28:137–166. https://doi.org/10.1016/S0301-9322(01)00055-6

Gadala-Maria F, Acrivos A (1980) Shear-induced structure in a concentrated suspension of solid spheres. J Rheol 24:799–814. https://doi.org/10.1122/1.549584

Ghisalberti M, Nepf H (2009) Shallow flows over permeable medium: the hydrodynamics of submerged aquatic canopies. Trans Porous Med 78:309–326. https://doi.org/10.1007/s11242-008-9305-x

Goharzadeh A, Khalili A, Jørgensen BB (2005) Transition layer thickness at a fluid-porous interface. Phys Fluids 17:057102. https://doi.org/10.1063/1.1894796

Goto H, Kuno H (1982) Flow of suspensions containing particles of two different sizes through a capillary tube. J Rheol 26:387–398. https://doi.org/10.1122/1.549682

Goyeau B, Lhuillier D, Gobin D, Velarde MG (2003) Momentum transport at a fluid-porous interface. Int J Heat Mass Transfer 46:4071–4081. https://doi.org/10.1122/1.549682

Guo P, Weinstein AM, Weinbaum S (2000) A hydrodynamic mechanosensory hypothesis for brush border microvilli. Am J Physiol Renal Physiol 279:698–712. https://doi.org/10.1152/ajprenal.2000.279.4.F698

Haffner EA, Mirbod P (2020) Velocity measurements of a dilute particulate suspension over and through a porous medium model. Phys Fluids 32:083608. https://doi.org/10.1063/5.0015207

Hampton RE, Mammoli AA, Graham AL, Tetlow N (1997) Migration of particles undergoing pressure-driven flow in a circular conduit. J Rheol 41:621–640. https://doi.org/10.1122/1.550863

Han M, Kim C, Kim M, Lee S (1997) Particle migration in tube flow of suspensions. J Rheol 43:1157–1174. https://doi.org/10.1122/1.551019

Jenkins JT, McTigue DF (1990) Transport processes in concentrated suspensions: the role of particle fluctuations. In: Schaeffer DG (ed) Joseph DD. Springer, Two Phase Flows and Waves, pp 70–79. https://doi.org/10.1007/978-1-4613-9022-0_5

Kang C, Mirbod P (2019) Porosity effects in laminar fluid flow near permeable surfaces. Phys Rev E 100:013109. https://doi.org/10.1103/PhysRevE.100.013109

Kang C, Mirbod P (2020) Shear-induced particle migration of semi-dilute and concentrated Brownian suspensions in both Poiseuille and circular Couette flow. Int J Multiphase Flow 126:103239. https://doi.org/10.1016/j.ijmultiphaseflow.2020.103239

Kang C, Yang KS (2011) Heat transfer characteristics of baffled channel flow. ASME J Heat Transfer 133:091901. https://doi.org/10.1115/1.4003829

Kang C, Yang KS (2012) Flow instability in baffled channel flow. Int J Heat Fluid Flow 38:40–49. https://doi.org/10.1016/j.ijheatfluidflow.2012.08.002

Karnis A, Goldsmith HL, Mason SG (1966) The kinetics of flowing dispersions: I. Concentrated suspensions of rigid particles. J Colloid Interface Sci 22:531–553. https://doi.org/10.1016/0021-9797(66)90048-8

Kim J, Moin P (1985) Application of a fractional-step method to incompressible Navier-Stokes equations. J Comp Phys 59:308–323. https://doi.org/10.1016/0021-9991(85)90148-2

Koh CJ, Hookham P, Leal LG (1994) An experimental investigation of concentrated suspension flows in a rectangular channel. J Fluid Mech 266:1–32. https://doi.org/10.1017/S0022112094000911

Krieger IM (1972) Rheology of monodisperse lattices. Adv Colloid Interf Sci 3:111–136. https://doi.org/10.1016/0001-8686(72)80001-0

Kruijt B, Malhi Y, Lloyd J, Norbre AD, Miranda AC, Pereira MGP, Culf A, Grace J (2000) Turbulence statistics above and within two Amazon rain forest canopies. Bound-lay Meteorol 94:297–331. https://doi.org/10.1023/A:1002401829007

Leighton D, Acrivos A (1987) The shear-induced migration of particles in concentrated suspensions. J Fluid Mech 181:415–439. https://doi.org/10.1017/S0022112087002155

Lyon MK, Leal LG (1998a) An experimental study of the motion of concentrated suspensions in two-dimensional channel flow. Part 1. Monodisperse system. J Fluid Mech 363:25–56. https://doi.org/10.1017/S0022112098008817

Lyon MK, Leal LG (1998b) An experimental study of the motion of concentrated suspensions in two-dimensional channel flow. Part 2. Bidisperse system. J Fluid Mech 363:57–77. https://doi.org/10.1017/S0022112098008829

Miller RM, Morris JF (2006) Normal stress-driven migration and axial development in pressure-driven flow of concentrated suspensions. J Non-Newton Fluid 135:149–165. https://doi.org/10.1016/j.jnnfm.2005.11.009

Mirbod P (2016) Two-dimensional computational fluid dynamical investigation of particle migration in rotating eccentric cylinders using suspension balance model. Int J Multiphase Flow 80:79–88. https://doi.org/10.1016/j.ijmultiphaseflow.2015.11.002

Mirbod P, Wu Z, Ahmadi G (2017) Laminar flow drag reduction on soft porous media. Sci Rep 7:17263. https://doi.org/10.1038/s41598-017-17141-3

Morris JF, Boulay F (1999) Curvilinear flows of noncolloidal suspensions: the role of normal stresses. J Rheol 43:1213–1237. https://doi.org/10.1122/1.551021

Morris JF, Brady JF (1998) Pressure-driven flow of a suspension: buoyancy effects. Int J Multiphase Flow 24:105–130. https://doi.org/10.1016/S0301-9322(97)00035-9

Nott PR, Brady JF (1994) Pressure-driven flow of suspensions: simulation and theory. J Fluid Mech 275:157–199. https://doi.org/10.1017/S0022112094002326

Phillips RJ, Armstrong RC, Brown RA (1992) A constitutive equation for concentrated suspensions that accounts for shear-induced particle migration. Phys Fluids A 4:30–40. https://doi.org/10.1063/1.858498

Rosti ME, Mirbod P, Brandt L (2021) The impact of porous walls on the rheology of suspensions. Chem Eng Sci 230:116178. https://doi.org/10.1016/j.ces.2020.116178

Sinton SW, Chow AW (1991) NMR flow imaging of fluids and solid suspensions in Poiseuille flow. J Rheol 35:735–772. https://doi.org/10.1122/1.550253

Subia SR, Ingber MS, Mondy LA, Altobelli SA, Graham AL (1998) Modelling of concentrated suspensions using a continuum constitutive equation. J Fluid Mech 373:193–219. https://doi.org/10.1017/S0022112098002651

Tachie MF, James DF, Currie IG (2004) Slow flow through a brush. Phys Fluids 16:445–451. https://doi.org/10.1063/1.1637351

Vafai K, Kim SJ (1990) Fluid mechanics of the interface region between a porous medium and a fluid layer-an exact solution. Int J Heat Fluid Flow 11:254–256. https://doi.org/10.1016/0142-727X(90)90045-D

Wu Z, Mirbod P (2018) Experimental analysis of the flow near the boundary of random porous media. Phys. Fluids 30:047103. https://doi.org/10.1063/1.5021903

Wu Z, Mirbod P (2019) Instability analysis of the flow between two parallel where the bottom one coated with porous media. Adv Water Resour 130:221–228. https://doi.org/10.1016/j.advwatres.2019.06.002